

Cite this: *Soft Matter*, 2012, **8**, 11123

www.rsc.org/softmatter

PAPER

# Modelling elasticity and memory effects in liquid crystalline elastomers by molecular dynamics simulations

Jaroslav M. Ilnytskyi,<sup>\*a</sup> Marina Saphiannikova,<sup>b</sup> Dieter Neher<sup>c</sup> and Michael P. Allen<sup>d</sup>

Received 28th June 2012, Accepted 1st August 2012

DOI: 10.1039/c2sm26499d

We performed molecular dynamics simulations of a liquid crystal elastomer of side-chain architecture. The network is formed from a melt of 28 molecules each having a backbone of 100 hydrocarbon monomers, to which 50 side chains are attached in a syndiotactic way. Crosslinking is performed in the smectic A phase. We observe an increase of the smectic–isotropic phase transition temperature of about 5 degrees as compared to the uncrosslinked melt. Memory effects in liquid crystalline order and in sample shape are well reproduced when the elastomer is driven through the smectic–isotropic transition. Above this transition, in the isotropic phase, the polydomain smectic phase is induced by a uniaxial load. Below the transition, in a monodomain smectic A phase, both experimentally observed effects of homogeneous director reorientation and stripe formation are reproduced when the sample is stretched along the director. When the load is applied perpendicularly to the director, the sample demonstrates reversible deformation with no change of liquid crystalline order, indicating elasticity of the two-dimensional network of polymer layers.

## I. Introduction

The combination of liquid-crystalline (LC) groups and a polymeric matrix is particularly appealing to the materials scientist, in view of the large number of applications which exist for both parent subsystems.<sup>1</sup> Moreover, composite systems of this type exhibit a synergy, *i.e.* the presence of properties not observed in their constituent parts. One such system, the liquid crystalline elastomer (LCE), combines the elasticity of a weakly crosslinked polymer network with the ordering abilities of covalently attached LC groups, and also the response of the latter to an external electromagnetic field.<sup>2</sup> Due to coupling between these two constituent subsystems, a number of opto- and thermo-mechanical effects are observed in LCEs, bringing them into the wider class of shape-memory polymers.<sup>3,4</sup> For instance, reversible shape changes at the LC order–disorder transition provide a basis for applications of LCE as low frequency actuators and sensors (*i.e.* artificial muscles).<sup>5,6</sup> A separate class of technologically interesting materials are LCEs with photo-sensitive (*e.g.* azobenzene) groups.<sup>7</sup>

One can classify the effects observed in LCEs under external stimuli on the basis of the physical nature of the latter. First we will review the effects connected with temperature change. For weakly crosslinked networks, the LC groups retain the ability to

form LC phases and the LC transition is the only principal change undergone by LCEs on varying the temperature (presuming the temperatures to lie above the glass transition temperature). Crosslinking stabilizes the LC phase in which the network is originally formed, due to memorizing the backbone conformations.<sup>8–11</sup> This is indicated by a rise of the order–disorder transition temperature, if crosslinking was performed in an ordered phase. On top of this, a number of memory effects are observed. In particular, the sample may be held at temperatures well above the nematic–isotropic transition for extended periods (two weeks), but on cooling into the liquid crystal phase region, the original monodomain order is recovered with the same director alignment.<sup>12</sup> This is in contrast to the case of an uncrosslinked sample of the same copolymer, in which case no retention was shown of the global orientation after holding the sample for 60 s in the isotropic state.<sup>12</sup>

The change of LC order upon cooling an LCE from the isotropic phase is accompanied by the deformation of the material along the director axis.<sup>13–18</sup> The effect is the consequence of the coupling between the average anisotropy of polymer chains and the nematic order parameter, and it has some specific features outlined below. Small-angle neutron scattering experiments on deuterium labeled mixtures have revealed that both types of backbone anisotropy, parallel and perpendicular to the director, are possible,<sup>19–21</sup> as well as switching between the two (reminiscent of the odd-even effect in nematics).<sup>22</sup> In this respect, positive and negative coupling coefficients are often used indicating that backbones are extended parallel or normal to the liquid crystal director, respectively. As remarked in ref. 23, for nematic polymers, typical ratios between radii of gyration of

<sup>a</sup>Institute for Condensed Matter Physics of National Academy of Sciences of Ukraine, 1, Svientsitskii Str., 79011 Lviv, Ukraine. E-mail: [iln@icmp.lviv.ua](mailto:iln@icmp.lviv.ua)

<sup>b</sup>Leibniz Institute of Polymer Research, 01069, Dresden, Germany

<sup>c</sup>Institute for Physics and Astronomy, University of Potsdam, Karl-Liebknecht-Strasse 24-25, 14476 Potsdam-Golm, Germany

<sup>d</sup>Department of Physics, University of Warwick, Coventry, CV4 7AL, UK

backbones parallel and perpendicular to the director,  $R_{\parallel}/R_{\perp}$ , are found to be close to 0.7 or 1.3. For smectic polymers, backbones are retained inside layers and  $R_{\parallel}/R_{\perp}$  is much smaller than one.<sup>24</sup> The arrangement of backbones has a profound effect on the deformation of the LCE when driven through the LC order–disorder transition. As pointed out in ref. 15, the magnitude of the uniaxial strain could differ greatly and even change sign from extension to contraction in a polymer with oblate backbone conformation. One should also take into account spatial repacking of bulky LC groups during the transition. Both contributions (from LC groups and backbones) may either add-on or compete when shaping out the final deformation of the sample.<sup>25,26</sup> In the case of main-chain nematic polymer systems, one has strong positive coupling between LC groups and backbones, and spontaneous reversible deformation with a strain of 3–4 can be achieved.<sup>27,28</sup>

Let us switch now to the opposite type of effect, in which a mechanical load is used as a driving stimulus. It has been realized since the early studies that in this way one can manipulate the LC order of the LCE.<sup>29–32</sup> A fundamental mechanism here is that an applied stress induces an anisotropy in the polymer backbone, which results in a macroscopic alignment of the director by virtue of coupling.<sup>16</sup> Due to this, the load induces remarkable changes in the structure of the LCE, if its axis is not collinear with the axis of initial anisotropy of backbones.

When applied to a polydomain sample, a uniaxial load is able to induce homogeneous LC order. This effect is used for fabrication of liquid single crystal elastomers *via* a two-stage cross-linking technique.<sup>23</sup> When applied to an initially ordered monodomain nematic LCE, it may change the already existing LC order.<sup>23,29,33</sup> In the case of positive LC–backbone coupling, the changes occur when the load axis is not collinear with the initial director, due to the arguments above. When the load is applied normally to the director, then the sample first turns opaque (accompanied by softening of the material) and then a monodomain sample is formed in which the director is parallel to the load.<sup>23</sup> The opaque state turns out to have a periodic pattern (more details are given below). Two issues can be emphasized here, namely, (i) the reorientation process sets in at a distinct threshold stress and (ii) the magnitude of the order parameter after completing the reorientation process is considerably below its initial value. The fine details of crosslinking are found to be important in this respect.<sup>34</sup> Later the study was extended to the case of arbitrary angle between the stress axis and director. Contrary to the case of normal angle (where the reorientation process sets in at a threshold strain and a periodic pattern formation is observed), at oblique angles, a uniform director reorientation is obtained with retention of the monodomain structure, and no threshold strain is observed.<sup>35</sup> Similar results were reported by Roberts *et al.*<sup>36</sup> The strain was applied nearly normal to the initial director and molecular rearrangement is accompanied by a decrease in nematic order parameter during the rotation. Wide-angle X-ray scattering and optical microscopy studies have revealed a single director orientation throughout the switching process; broad optical-texture variations are observed after the director flip has occurred, although the sample remains optically clear throughout the process.<sup>36</sup> The director reorientation in nematic LCEs is extensively discussed theoretically.<sup>37–41</sup>

So far we briefly reviewed experimental work covering relevant properties of nematic LCEs; however, much less work has been done on their smectic A counterpart. It was found<sup>42</sup> that macroscopically uniformly aligned smectic A LCEs are characterized by a highly anisotropic solid-like response, with an elastic constant along the layer normal about two orders of magnitude larger than that in the layer plane. As far as the Sm A phase is characterized by negative backbone–LC coupling, then stress-driven changes in LC order are expected when the sample is stretched along the layer normal (parallel to the director). If the load is applied in this way and it exceeds a threshold value, then a breakdown of the monodomain structure is observed resulting in a completely turbid sample<sup>42</sup> suggesting layer undulation (see Fig. 14 in ref. 43). When the sample is deformed parallel to the layers, it stays clear up to high strains of 200%, and maintains its full width in the direction parallel to the layer normal.<sup>42</sup> Besides these experimental studies, much effort has been made to investigate strain-induced changes in LCEs theoretically. For example, Stenull and Lubensky have developed a theory which predicts the strain-induced transition from the smectic A to smectic C phase, which is accompanied by a change in the elastic modulus.<sup>44</sup> Another group of researchers put forward the concept of soft elasticity, when the plateau in the stress–strain curves of smectic LCEs has been explained as an ability of the LCE to deform at no energy cost.<sup>45,46</sup> Such a deformation can be performed by rotation of the nematic director and is characterized by a vanishing value of the elastic modulus.<sup>2</sup>

As remarked in ref. 47, one of the most striking phenomena is the formation of textured deformations as a response of a homogeneous monodomain LCE to a macroscopically homogeneous imposed strain.<sup>35,48</sup> This behavior can be explained in a way that when the LCE is stretched and the nematic director rotates, the energy of the deformation is much reduced if the elastomer also shears. The sample is split into stripes that alternate between equal and opposite director rotation and shear.<sup>37,47,49</sup> This scenario is especially true for smectic LCEs, that are layered, and there is a large energy penalty associated with causing the director to deviate from the smectic layer normal or changing the inter-layer spacing.<sup>45</sup> Fried and Sellers showed that the postulated director rotations and shears in the domain regions do not necessarily confirm soft elasticity, but are also predicted by more general constitutive models that do not involve any notion of softness.<sup>50</sup> The uniform director rotation *vs.* patterned stripes scenario when the LCE is stretched perpendicularly to the director may also depend on the details of sample preparation.<sup>51</sup>

In contrast to the vast amount of experimental and theoretical research outlined above, computer simulation studies for LCE systems are rather scarce. These, to the best of our knowledge, are done for continuum models,<sup>52</sup> lattice models<sup>53–56</sup> and off-lattice models for side-chain<sup>57,58</sup> and main-chain LCEs.<sup>59,60</sup> However, computer simulations have obvious benefits in that all the movements of particles can be traced, enabling direct study of backbone anisotropy, LC order, and coupling effects between the two. Difficulties associated with this approach are linked to the fact that elastic properties of the network appear on a length-scale rather large compared to that of the atoms and, therefore, relatively large model system sizes are needed.

The current study can be seen as a continuation of our previous research on the properties of uncrosslinked side-chain LC polymers, namely on their statics and dynamics in various phases<sup>24</sup> as well as on photo-induced deformations for the case of azobenzene-containing systems.<sup>25,26</sup> A semi-atomistic model is used, similar to those from ref. 24, but with longer backbone; the crosslinking is performed in the Sm A phase. The crosslinked melt is compared side-by-side with the uncrosslinked one, which serves as a reference system. Molecular dynamics (MD) simulations are performed in the anisotropic isobaric ensemble with the aid of the GBMOLDD program.<sup>61,62</sup> We aim to demonstrate that the principal features of LCEs, such as memory effects in both the LC order and sample shape, as well as stress-driven manipulation of LC order, are reproduced within a model system of moderate size.

Practically reasonable system sizes for atomic-resolution simulations of LC melts and networks lie within the 10–100 nm range, well below the typical dimensions of real physical samples that demonstrate elasticity. In this context, the issue arises of how phenomena occurring at smaller length scales in such a material influence its macroscopic behaviour. As discussed in ref. 63 and 64, at the micro-level the material response is heterogeneous, whereas at the macro-level it appears homogeneous. One could explain this by averaging the material properties over a large number of inhomogeneous fragments (in the same way that “self-averaging” applies to the description of disordered critical systems<sup>65</sup>).

One can attempt to mimic larger system behaviour from the simulation of a smaller one by some reduction of both the number and the length-scale of the inhomogeneities. To this end we use here a dense comb architecture and perform crosslinking in a controlled way. In some cases we analyze several independently prepared samples. In any case, this study assumes the affine deformation property for this particular system which allows one to extrapolate the deformation of a small sample onto a macroscopic system. Our system sizes (greater than  $10^4$  particles) are typical of those used elsewhere to simulate LC elastomers (see *e.g.* ref. 60). More discussion on the computational approaches addressing the relationship between micro- and macro-scales in composite systems can be found elsewhere.<sup>64,66</sup>

The outline of this paper is as follows. The details of the modeling and simulation technique are provided in Section II, the formation of the network and the smectic–isotropic transition are discussed in Section III, memory effects are covered in Section IV, and stress-driven transformations are considered in Section V. Conclusions are given in Section VI.

## II. Molecular model and preparation of a pre-crosslinked melt

In this study we use a hybrid force-field model, in which polymer monomers are described *via* spherical united atoms, and the mesogens *via* rigid prolate bodies.<sup>67</sup> The flexibility of the polymer chains is governed by torsional potentials, whereas the ability of the LC groups to form ordered phases is controlled *via* parameters of the mesomorphic Gay–Berne potential.<sup>68</sup> This approach is found to be successful for simulations of a wide range of LC polymer architectures.<sup>24,26,69–75</sup> The details of the force field being used can be found elsewhere.<sup>24,61,62</sup>

The MD simulations are performed with the aid of the parallel program GBMOLDD.<sup>61,62</sup> A simulation box of the dimensions  $L_x$ ,  $L_y$  and  $L_z$ , with periodic boundary conditions, that mimicks the behavior of a volume element in the bulk, is used. We employed the  $NP_{xx}P_{yy}P_{zz}T$  ensemble, that is a simplified version of the Parrinello–Rahman ensemble,<sup>76</sup> in which only the principal stresses  $\sigma_{xx}$ ,  $\sigma_{yy}$ ,  $\sigma_{zz}$  are constrained (the equations of motion can be found in ref. 24). Two types of simulation are undertaken in this study: under atmospheric pressure,  $P_{\text{atm}}$  and under external uniaxial load. In the first case all three principal stresses are constrained at the same value of  $P_{\text{atm}}$ . In the second case, a load  $P_L$  is introduced along one of the axes,  $\alpha = \{x, y, z\}$ , by constraining  $\sigma_{\alpha\alpha}$  to  $P_{\text{atm}} - P_L$ , whereas both other stresses,  $\sigma_{\beta\beta}$  and  $\sigma_{\gamma\gamma}$ , are constrained at  $P_{\text{atm}} + P_L/2$ . In this way the trace of the stress tensor is always equal to  $3P_{\text{atm}}$ . For the integration of the equations of motion we used the leap-frog algorithm; the RATTLE constraint has been applied for the integration of the mesogen rotation (see ref. 62). The time step  $\Delta t = 2$  fs was found to be acceptable for all production runs.

Anisotropic deformation of the simulation box at each time instant  $t$  is monitored *via* the three principal strains,  $\varepsilon_\alpha = L_\alpha(t)/L_\alpha(0)$ , where  $L_\alpha(t)$  is a dimension of the box along the corresponding spatial axis  $\alpha$  at time  $t$ . We usually define these strains such that uniaxial symmetry applies along the  $Z$  axis (*e.g.* nematic director, axis of applied load, *etc.*), therefore,  $\varepsilon_z$  is referred to as  $\varepsilon$  to simplify notation.

To characterize the LC order of the mesogens, we evaluate the nematic order parameter with respect to the director,  $S_2$ , and also the order parameters  $S_\alpha$  evaluated with respect to each spatial axis  $\alpha$ :

$$S_2 = \langle P_2(\cos(\theta_i)) \rangle_i, S_\alpha = \langle P_2(e_i^\alpha) \rangle_i. \quad (1)$$

Here  $P_2$  is a Legendre polynomial, and  $\theta_i$  is the angle between  $e_i$  and the nematic director, where  $e_i$  is a unit vector representing the orientation of the  $i^{\text{th}}$  mesogen in space;  $e_i^\alpha$  is the component of  $e_i$  along the  $\alpha$  axis.<sup>61</sup> The averaging is performed over all the mesogens within the system.

As a practical measure of backbone anisotropy with respect to a certain axis  $\alpha$  (*e.g.* director, axis of applied load, *etc.*) we use the ratio between the averaged radii of gyration parallel,  $R_{\parallel}$ , and normal,  $R_{\perp}$ , to this axis:

$$\frac{R_{\parallel}}{R_{\perp}} = \frac{\sqrt{G_{\alpha\alpha}}}{(\sqrt{G_{\beta\beta}} + \sqrt{G_{\gamma\gamma}})/2}, \quad (2)$$

where  $\beta$  and  $\gamma$  stand for the two directions perpendicular to  $\alpha$ . The averaging of the components of gyration tensor,  $G_{\alpha\beta}$ , is performed over all molecules of the melt (network), where the respective components for each molecule  $k$  are:

$$G_{\alpha\beta}^{[k]} = \frac{1}{N} \sum_{i=1}^N (r_{i,\alpha}^{[k]} - R_\alpha^{[k]}) (r_{i,\beta}^{[k]} - R_\beta^{[k]}). \quad (3)$$

Here  $i$  indexes the backbone site within molecule  $k$  and  $R^{[k]}$  is the position of the backbone center of mass. Implicit in the above equations is that the principal axes of the gyration tensor coincide with the box axes, which is the case here.

The minor changes in overall density of the system observed in our simulations, especially at the order–disorder transition, are

attributed to excluded volume issues associated with the mesogens.<sup>77,78</sup> These can be considered as unimportant in the context of elastic properties of the LCEs studied here, and are not emphasized in the following discussion.

The pre-crosslinked system is a melt of LC macromolecules of side-chain architecture. To promote formation of a network with a minimal number of crosslinks, we use molecules with a relatively long backbone of 100 spherical sites. 50 side chains are attached to the backbone in a syndiotactic way (hence, the functionality is two). Of these, 40 side chains have a spacer of six sites and are terminated by the mesogen (shown in Fig. 1 as a magenta-colored prolate body). The remaining 10 side chains have a spacer of four sites and are terminated by a chemically active site (shown in blue) which is intended for future crosslinking. At first, one molecule is formed by attaching both types of chains randomly to the backbone branching sites (see Fig. 1). Then, 28 replicas of the molecule are generated. Each molecule contains in total 380 spherical and 40 LC sites. The same force field parameters are used as in ref. 24 and, therefore, these are not repeated here. The melt of these molecules will be denoted here and thereafter as an “LCP melt”.

Preparation of the initial configuration for the LCP melt is performed in the same way as described in ref. 24 for the side chain LC polymer with similar architecture.  $N_{\text{mol}} = 28$  molecules are packed into the simulation box in a regular geometric way with a density of  $\rho = 0.8 \text{ g cm}^{-3}$ . The typical box size is about 100 Å. This configuration is heated up to  $T = 800 \text{ K}$  for 4 ns to erase any memory of the initial spatial arrangement (see frame (a) of Fig. 2). Formation of a monodomain LC phase is aided by an external field which acts on each mesogen and is defined *via* the following additional energy term:

$$U_i^{\text{rot}} = -F \cos^2(\varphi_i), \quad (4)$$

where  $\varphi_i$  is the angle between the long axis of the  $i^{\text{th}}$  mesogen and the direction of the field, and  $F = f \times 10^{-20} \text{ J}$  where  $f$  is the reduced field strength. In this study we simultaneously reduce the temperature down to  $T = 450 \text{ K}$  and switch on the external field with reduced strength  $f = 0.4$ . No nematic phase is found, in agreement with typical experimental phase diagrams for the side-chain architecture with a spacer length of six hydrocarbons,<sup>79</sup> but the monodomain smectic phase is formed in about 12 ns. Then the field is switched off and the phase is found to be stable for at least 30 ns if kept at  $T = 450 \text{ K}$ . The lamellar structure of the resulting relaxed phase is depicted in frame (b) of Fig. 2. Several independent attempts (started from isotropic samples with different preparation history) always resulted in the formation of

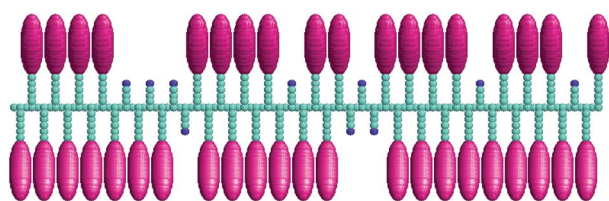


**Fig. 1** Schematic representation of a single molecule that forms the pre-crosslinked melt. Gray spheres: polymer pseudo-atoms ( $\text{CH}_n$ ). Magenta ellipsoids: mesogen groups. Free ending side chains are intended for future crosslinking (blue spheres: chemically active pseudo-atoms).

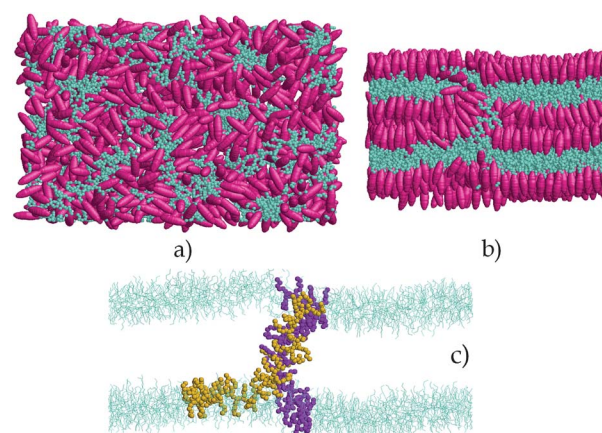


**Fig. 2** Isotropic phase of the LCP melt at 800 K (frame (a)) and monodomain smectic phase (frame (b)) grown *via*: (i) cooling this isotropic phase down to 450 K with simultaneous application of an external field eqn (4) with  $f = 0.4$ ; and (ii) consequent equilibration of the obtained smectic phase with no field applied. Irregularity in the form of a link between two lamellae (linking molecules are space filled and marked by color) is shown in frame (c).

the smectic phase with certain irregularities of their lamellar structure. In particular, the sample shown in frame (b) of Fig. 2 has a link between two polymer-rich lamellae formed by two molecules arranged parallel to the layer normal, as shown in frame (c) of the same figure. This is in contrast to the similar polymer considered in ref. 24 with much lower molecular weight, but consistent with the trend for high molecular weight chains in real-life, where such interlamellar links are widely expected (see, for example, Fig. 3 in ref. 43).

### III. Formation of a network and influence of crosslinking on the smectic–isotropic transition

In our modelling approach to produce the monodomain LCE sample, we followed one of the known experimental routes. In particular, as explained in ref. 33, a monodomain structure was created by holding a cast film of the polymer, containing the crosslinking agent, in the nematic phase range at 391 K, in a uniform magnetic field of 0.6 T within a protective nitrogen atmosphere. A monodomain structure was obtained within minutes. Simultaneously, crosslinking occurred through a thermally activated chemical reaction involving the hydroxyl sites in the copolymer and the crosslinking agent.<sup>10,12,16</sup>

The pre-crosslinked model LCP melt is prepared, as explained in Section II, using the similar approach of an orientating field applied to the mesogens (see eqn (4)). Ideally, one would be aiming at the formation of a single network molecular topology with the minimum number of crosslinks  $N_{\text{cl}}$  being equal at least to  $N_{\text{mol}}$ . This, however, faces certain difficulties due to the lamellar structure of the smectic phase and restricted mobility of chemically active sites. To avoid disruption of the initial smectic structure we opted to use “rubber band” crosslinks of about 4 Å in length that are longer than true “chemical” bond lengths (*e.g.*  $\sim 1.54 \text{ Å}$  for hydrocarbons) instead of forcing reactive sites into closer contact. The crosslink algorithm consists of the following steps:

(1) the list of pairwise distances between chemically active sites (that belong to different molecules) is built;

(2) this list is re-sorted in such a way that the pairs with smaller separation appear at the top, and the bottom of the list is cut at threshold value  $r_{\max} \sim 10 \text{ \AA}$ ;

(3) the simulation box of volume  $V$  is decomposed spatially into domains with the volume of each domain close to the volume per crosslink  $V/N_{\text{cl}}$ ;

(4) a loop is performed over all the domains, and for each domain we search for the topmost pair (if any) on the list, and if the pair is found it is registered as a crosslink and excluded from further processing.

(5) the bond lengths of all the crosslinks are set equal to a certain value  $\ell_{\text{cl}}$  and the crosslinked system is equilibrated to bring crosslink separations close to this value.

In short, this algorithm forces a more-or-less homogeneous distribution of the crosslinks within the simulation box, and prefers the least separated pairs to be crosslinked in the first place.  $N_{\text{cl}} = N_{\text{mol}} = 28$  crosslinks are made, where the initial separation between crosslinked sites ranged between  $3.5 \text{ \AA}$  and  $7.5 \text{ \AA}$ ; therefore the fixed “rubber band” value  $\ell_{\text{cl}} = 4.0 \text{ \AA}$  was chosen. Relaxation of the freshly linked network causes, therefore, none or minimal disruption to the initial smectic structure. In our particular sample we achieved a mixture of subnetworks of 18, 6, 2, 1 and 1 molecules in each. One should remark that real networks are also prone to various defects and inhomogeneities such as dangling chains, loops, trapped entanglements, *etc.*<sup>80–82</sup> Due to the multiple network structure of our LCE, we aim to observe the tendencies in changes of the LCP melt properties acquired as the result of (partial) crosslinking. These can be extrapolated further to predict the behavior of a single, fully crosslinked network.

Crosslinking, in general, stabilizes the LC phase in which it has been performed,<sup>8–11</sup> hence, we would expect a shift of the smectic–isotropic (SI) transition temperature towards higher values as compared to the case of the LCP melt. The exact amount of this shift depends on crosslink density, nematic order, and other factors<sup>9</sup> but is, typically, a few °C for weakly crosslinked LCEs. One also needs to take into account that, in contrast to low-molecular-weight LC materials, the order–disorder phase transition in LCEs is more smeared. The isotropic–nematic coexistence over a broad temperature range suggests that the heterogeneity in the samples introduces a distribution of transition temperatures.<sup>51</sup> Therefore, one might refer rather to a certain “transition region”, which defines an approximate interval for the SI transition temperature,  $T_{\text{SI}}$ . This interval is estimated from a series of heating runs performed at a range of temperatures, each run started from the same smectic sample being equilibrated at 450 K for at least 10 ns. The evolution of the order parameter  $S_2$  is shown in Fig. 3 for both cases of LCP melt and LCE. The transition region is found to be [500, 505] K for the melt and [505, 510] K for the elastomer, respectively. Therefore, the estimated increase of the transition temperature due to crosslinking of the melt is about  $\sim 5 \text{ °C}$ , in agreement with typical experimental findings.<sup>8–11</sup>

The SI transition is accompanied by a contraction of the simulation box along the initial director ( $Z$  axis). The amount of contraction is monitored *via* the uniaxial strain  $\epsilon = L_z/L_z(0)$  and is comparable for both cases of melt and network, being of the

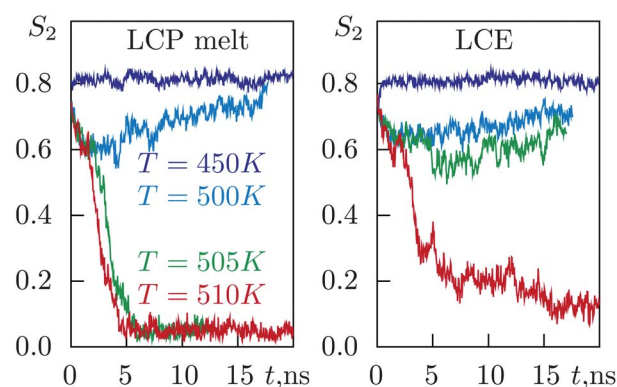


**Fig. 3** Evolution of the nematic order parameter for the LC groups in the LCP melt (left frame) and in the LCE (right frame) upon heating the initial smectic sample equilibrated at  $T = 450 \text{ K}$  up to higher temperatures (the temperatures are indicated in the left frame of the plot).

order of 0.8, see Fig. 4. Experimentally, a wide range of strain values have been observed, from 0.29 (ref. 15) to 0.95.<sup>16,33</sup> The exact amount in each case can be explained by the interplay of the sign of director–backbone coupling and the level of backbone anisotropy.<sup>15</sup> The latter is expected to depend on the molecular weight and rigidity of the backbone itself. In the case of our model, in the smectic phase, backbones are found in oblate conformations with the gyration tensor component along the director,  $G_{zz} \approx 60 \text{ \AA}^2$ , significantly smaller than either of the perpendicular components:  $G_{xx} \approx 700 \text{ \AA}^2$  and  $G_{yy} \approx 270 \text{ \AA}^2$ . Upon isotropization of the system, mesogens change their orientations to random ones, hence contributing to contraction of the sample along the initial director axis. The backbones spread from an oblate shape to random coil conformations with  $G_{xx} \approx 600 \text{ \AA}^2$ ,  $G_{yy} \approx G_{zz} \approx 300 \text{ \AA}^2$  and, therefore, contribute to the extension of the sample along the same axis. The net effect is the result of the competition between these two. For the particular model used in our study, the effect of mesogen reorientation provides a stronger contribution, resulting in a moderate contraction of the sample along the initial director axis.

Despite many similarities between the cases of LCP melt and LCE in terms of deformation upon entering the isotropic phase,

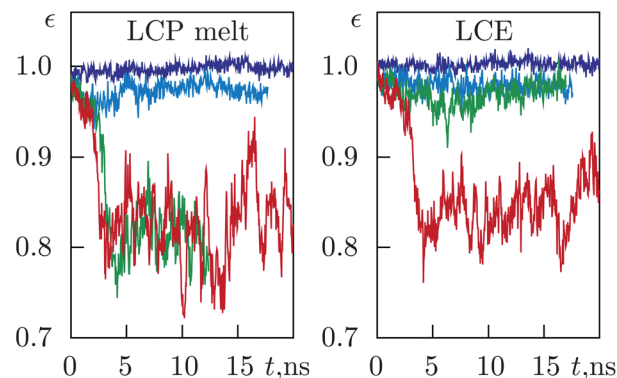


**Fig. 4** The uniaxial strain of the sample  $\epsilon = L_z/L_z(0)$  along the initial nematic director in the case of the LCP melt (left frame) and of the LCE (right frame) that occurs during the SI transition (temperatures are color coded in a similar way as in Fig. 3).

both systems demonstrate quite different attitudes towards the shape memory effects; this is considered in detail in the following section.

#### IV. Memory effects

Now we will turn our attention to the reversibility of the orientational order, and of the sample shape, when the LCE is driven on a temperature scale back and forth through the order-disorder transition. These thermo-mechanical memory effects, observed experimentally,<sup>12,33</sup> form a basis for possible technological applications of LCEs as artificial muscles.<sup>5,6</sup>

We first attempted to drive both systems (melt and elastomer) through the SI transition within an interval of  $T \in [500, 510]$  K. This turned out to be quite impractical due to the smeared transition (already mentioned above), massive pretransitional fluctuations and, as a result, extremely long relaxation times. However, memory effects are observed clearly and unambiguously when both systems are driven from rather deep in the smectic phase, at  $T = 450$  K, to the isotropic phase, at  $T = 510$  K, and back.

To this end we performed a set of runs started from the initial smectic phase  $S^{(0)}$  that is equilibrated at 450 K. This phase first is subjected to annealing at 510 K for a total time of about 40 ns. The intermediate isotropic phases that appear after 4 ns, 12 ns, 20 ns and 28 ns are labelled  $I^{(1)}$ ,  $I^{(2)}$ ,  $I^{(3)}$  and  $I^{(4)}$ , respectively. After this we perform quenching of all of these phases at  $T = 450$  K for at least 20 ns. The phases obtained as the result of quenching are marked as  $S^{(1)}$ ,  $S^{(2)}$ ,  $S^{(3)}$  and  $S^{(4)}$ , respectively. This is illustrated in Fig. 5 (top frame). Let us concentrate on the behavior of the mesogen order parameter  $S_2$  first; the results for both cases of LCP melt and LCE are shown in Fig. 5. One can see that both systems behave quite similarly, namely, that the order parameter for  $S^{(1)}$ – $S^{(4)}$  equals that of the initial phase  $S^{(0)}$ . This indicates that the LC subsystem self-assembles back into the smectic phase as the result of quenching (one should note the faster recovery of the LC order in the LCE case).

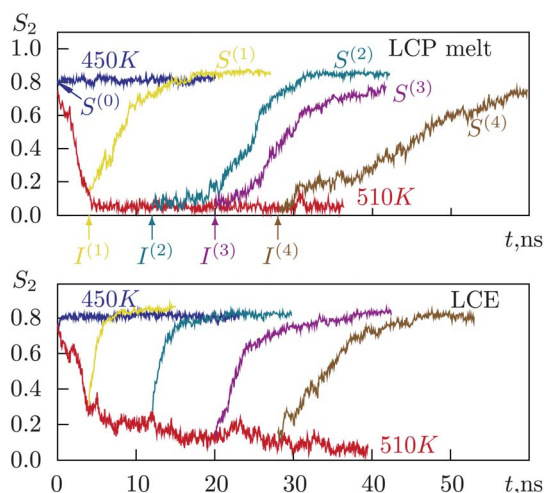


**Fig. 5** Evolution of the nematic order parameter  $S_2$ , eqn (1), for the LCP melt (top frame) and LCE (bottom frame) during the annealing run at  $T = 510$  K (red curve) and quenching runs at  $T = 450$  K (coloured curves). The latter are performed for each intermediate isotropic phase  $I^{(1)}$ – $I^{(4)}$  and result in self-assembly into smectic phases  $S^{(1)}$ – $S^{(4)}$ , respectively.

The shape of the simulation box upon quenching, however, behaves rather differently. The evolution of the uniaxial strain  $\epsilon$  along the axis of the initial nematic director is shown in Fig. 6. For the case of the LCP melt (top frame) the strain is reversible for the  $I^{(1)} \rightarrow S^{(1)}$  quenching run only. In contrast, in the case of LCE (bottom frame), the initial strain fully recovers for all quenching runs  $I^{(k)} \rightarrow S^{(k)}$ ,  $k = 1$ –4. The evolution of the order parameter and that of the strain upon quenching are found to be fully synchronized in this case.

This difference in reversibility of the smectic structure upon annealing/quenching runs in the LCP melt and LCE can be interpreted by significant hampering of diffusion in the latter case. First of all, this argument is supported by visual inspection of the snapshots obtained in annealing  $S^{(0)} \rightarrow I^{(3)}$  and quenching  $I^{(3)} \rightarrow S^{(3)}$  runs, see Fig. 7 and 8. In the case of the LCP melt (Fig. 7), the lamellar structure of the polymer in the  $I^{(3)}$  phase is already lost (middle row) and the arrangement of layers in the  $S^{(3)}$  phase (bottom frame) is different from that in the  $S^{(0)}$  phase (top frame). In contrast, in the case of the LCE (Fig. 8), the  $I^{(3)}$  phase preserves the essentials of the layering structure of the  $S^{(0)}$  phase, despite the layers being bent and distorted. This memory effect of the polymer matrix must play the principal role in a quick rebuild of an exact replica of the initial smectic structure found in the  $S^{(3)}$  phase (Fig. 8).

To quantify the rate of lamellar displacement during the annealing of the  $S^{(0)}$  phase (red curves in Fig. 5 and 6), we evaluated the mean-square displacement of polymer beads along the layer normal ( $Z$  axis):

$$g_{1,z}(t) = \langle (z_i(t) - z_i(0))^2 \rangle \quad (5)$$

where  $z_i(t)$  is the  $Z$  coordinate of the  $i^{\text{th}}$  polymer bead at time  $t$ , and averaging is performed over all beads; the zero of time is taken to be the start of the annealing process. An effective “diffusion coefficient”  $D_{1,z}(t)$  may be defined as half of the slope of this curve (although strictly this only applies for a system at

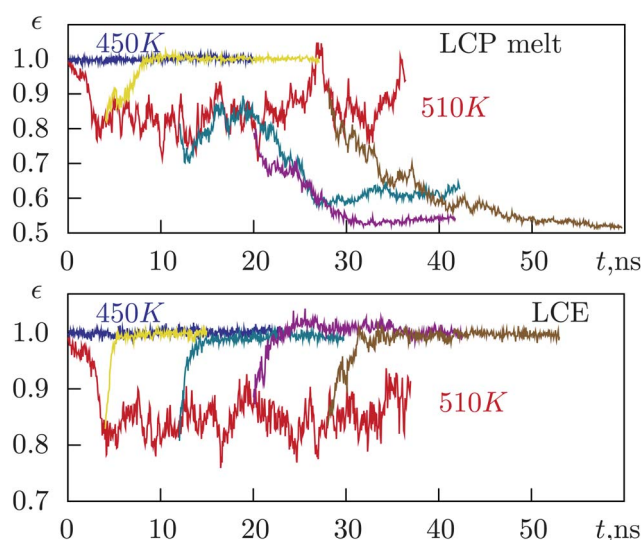


**Fig. 6** Evolution of the uniaxial strain  $\epsilon = L_z/L_z(0)$  along the axis of the initial nematic director for the LCP melt (top frame) and LCE (bottom frame) in quenching runs. The same color-coding applies as in Fig. 5.

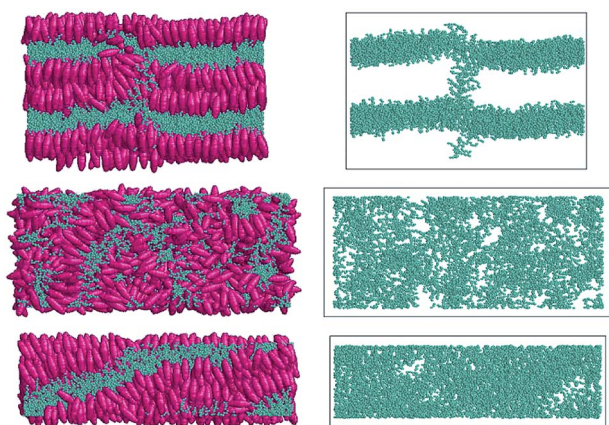


**Fig. 7** The sequence of snapshots that demonstrates the changes undergone by a polymer matrix of LCP upon an annealing/quenching cycle. Top row: initial smectic phase  $S^{(0)}$ ; central row: isotropic phase  $I^{(3)}$ ; bottom row: recovered smectic phase  $S^{(3)}$  (these phases are introduced in the text and can also be identified in Fig. 5). In each row both polymer and LC subsystems are shown on the left, and the polymer subsystem alone on the right.

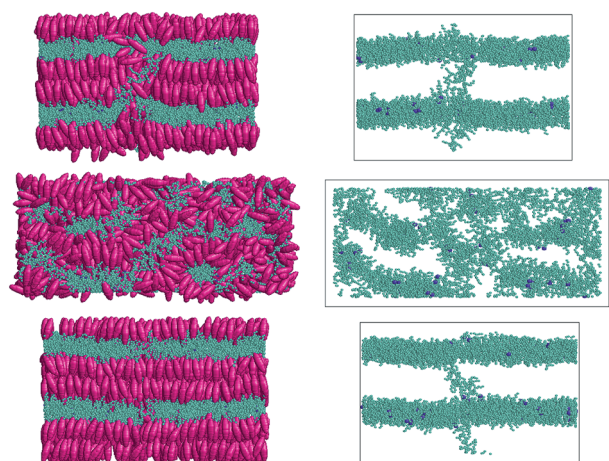


**Fig. 8** The sequence of snapshots that demonstrates the changes undergone by a polymer matrix of LCE upon an annealing/quenching cycle. The same arrangement of the snapshots is used as described in Fig. 7. Crosslinked sites are shown in blue.

equilibrium). The results are presented in Fig. 9, and several conclusions can be drawn from these. The first is that  $D_{1,z}$  at times above  $\sim 30$  ns is similar for both cases of LCP melt and LCE. One may suggest that, on this time scale, the effect of crosslinking seems to vanish for our particular sample. However, on a shorter time scale  $t < 30$  ns, there is a marked difference between both. Indeed, the estimate for  $D_{1,z}$  made within the interval  $t \in [0, 30]$  ns (marked by dashed lines in Fig. 9) is  $29.1 \text{ \AA}^2 \text{ ns}^{-1}$  for the LCP melt vs.  $9.1 \text{ \AA}^2 \text{ ns}^{-1}$  for the LCE. This quantifies a significant slowing down of the polymer dynamics as the result of crosslinking within a time interval below 30 ns.

Concerning the memory effects, one could suggest that above a certain threshold value for the mean square displacement,  $g_{1,z}^{\max}$ , the memory of the initial lamellar structure is lost. A rough estimate of  $g_{1,z}^{\max} \approx 700 \text{ \AA}^2$  can be made from Fig. 9, taking into

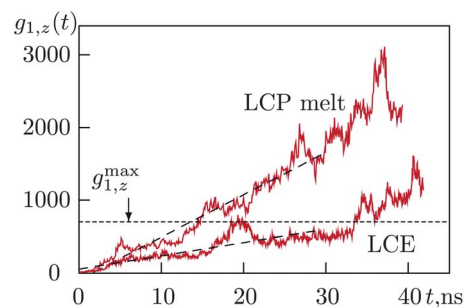


**Fig. 9** Mean square displacements for polymer beads along the  $Z$  axis,  $g_{1,z}(t)$ , during the transition of the initial smectic phase into the isotropic one *via* heating the latter up to  $T = 510$  K. Both cases of LCP melt and LCE are marked in the figure. Effective diffusion coefficients  $D_{1,z}$  are estimated by linear interpolation over the time interval  $t \in [0, 30]$  ns (marked by dashed lines).  $g_{1,z}^{\max}$  is an estimate for the maximum mean-square displacement at which deformation of lamellae is irreversible and the initial smectic structure is not retrieved upon cooling the system back to  $T = 450$  K.

account that the shape reversibility of the LCP melt is lost within the  $t_{\text{th}} \in [4\text{--}12]$  ns interval (see Fig. 6). We draw a horizontal dashed line for  $g_{1,z}^{\max}$  which crosses the  $g_{1,z}(t)$  curve for the LCP melt at approximately  $t = 14$  ns. One indirect confirmation of this estimate is that the corresponding displacement is  $\approx 26.5 \text{ \AA}$  which is of the order of the lamellar pitch for the  $S^{(0)}$  phase. Another confirmation is that the linear interpolation for the  $g_{1,z}(t)$  curve in the case of the LCE reaches  $g_{1,z}^{\max}$  at  $t > 30$  ns. This correlates well with the time window where the memory is preserved in this case (see Fig. 6). One can conclude that the time window for reversibility of the smectic order in the annealing/quenching cycle is defined by the diffusion rate of the polymer matrix and is, therefore, different, in the LCP melt and the LCE due to the effect of the crosslinks.

## V. Stress-driven transformations

Mechanical deformations applied to the LCE in the isotropic or in an ordered (nematic or smectic) phase give rise to a number of interesting effects as already reviewed in Section I.

First of all, purely mechanical properties of an LCE can be studied. In the isotropic phase, the LCE should possess an isotropic elasticity of the ordinary elastomer, whereas the elastic modulus in the smectic phase is known to be significantly anisotropic.<sup>42</sup> However, we found it a nearly impossible task to estimate a modulus from the stress–strain curves, the main obstacle being large fluctuations of the stress–tensor components (this can be attributed to the relatively small system size). On the other hand, indirectly measuring the elasticity, *via* a simulated creep experiment, turned out to be more successful. To do so, we impose a uniaxial external load  $P_L$  (as already explained in Section II) and monitor the shape for the uniaxial deformation of the box under load. The stress threshold is estimated approximately, by tabulating the load  $P_L$ .

The changes in LC order undergone by the LCE upon application of a uniaxial load are studied in both isotropic and smectic phases. In fact, the polydomain-to-monodomain transition can be induced in the globally isotropic phase.<sup>23,42,83</sup> In the smectic

phase, the load is applied both parallel and perpendicular to the nematic director; the aim is to reproduce a uniform and/or striped director reorientation, as observed experimentally and much discussed theoretically (for references, see Section I). The subsections below cover the cases of isotropic and smectic LCE samples subject to various uniaxial loads  $P_L$ .

### A. Isotropic phase: network elasticity and stress-induced disorder–order transition

In this subsection we present the results of a creep experiment applied to both systems (LCP melt and LCE) in the isotropic phase. Both isotropic samples were well equilibrated by heating the smectic sample up to  $T = 510$  K and keeping it at that temperature for 34 ns (*i.e.* somewhat longer than for the intermediate isotropic phase marked as I<sup>(4)</sup>, see Fig. 5). Uniaxial loads in the range  $P_L = 10$ –37 atm are applied along the Z axis for 48 ns. For the case of  $P_L = 37$  atm, we performed an additional run in the time interval  $t \in [48$  ns, 90 ns] in which the load was released.

The evolution of a uniaxial deformation  $\epsilon = (L_z(t) - L_z(0))/L_z(0)$  as the result of creep is shown in Fig. 10. The LCP melt behaves in a purely viscous manner until it eventually fractures (indicated by “x” symbols) before any changes in the LC order can be induced. In contrast, the crosslinked LCE demonstrates a considerable amount of elasticity. One can distinguish two regimes: (i) a viscous regime ( $t < t^*$ ), and (ii) an elastic regime ( $t > t^*$ ), where the deformation saturates at a value of 500–800% depending on  $P_L$ .

Let us concentrate on the case of  $P_L = 37$  atm, for which we studied the behavior of the mesogen order parameter  $S_\alpha$ , eqn (1), with respect to each spatial axis  $\alpha$ , and also the anisotropy of the backbone radius of gyration  $R_{\parallel}/R_{\perp}$ , eqn (2) with the parallel component evaluated along the stress axis Z. The results are shown in Fig. 11. One can observe that in the viscous regime  $t < t^* \approx 20$  ns the backbone anisotropy increases sharply (which results in an increase of the deformation along the load axis,  $\epsilon$ , as seen in Fig. 10). At the end of this regime the mesogens follow the spatial redistribution of the backbones; this is indicated by the changes in their order parameters  $S_\alpha$ . An ordered phase with

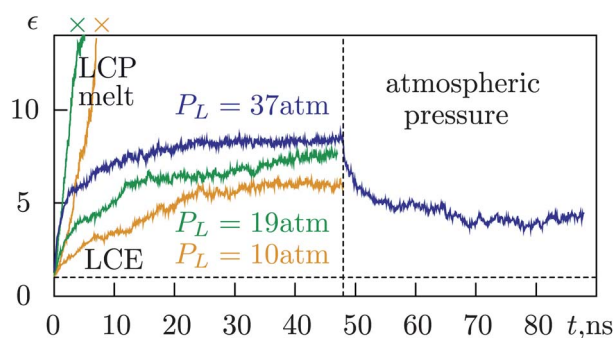


**Fig. 10** Uniaxial strain  $\epsilon$  along the Z axis, as a result of loads of various strengths  $P_L$  applied in that direction to the initially isotropic samples at 510 K. For the case  $P_L = 37$  atm an additional run is performed in which the load was released at  $t = 48$  ns and the system kept at atmospheric pressure. The cases of LCP melt and LCE are indicated in the figure; × symbols mark fracturing of the material.

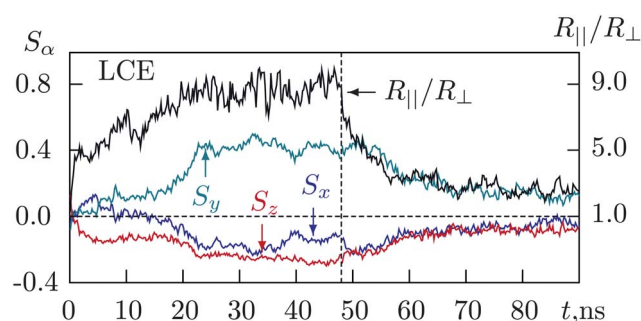


**Fig. 11** Nematic order parameter  $S_\alpha$  along each spatial axis  $\alpha$ , and backbone anisotropy  $R_{\parallel}/R_{\perp}$ , at load  $P_L = 37$  atm applied along the Z axis to the LCE at  $T = 510$  K.

order parameter  $S_y \approx 0.4$  is formed along the Y axis. One can deduce that considerable backbone anisotropy of at least 5–6 is required to initiate formation of this ordered phase. On release of the stress, the order and the deformation of the LCE moves back towards the pre-deformational initial state, but a residual backbone anisotropy of about 2.5–3, and residual order of  $S_y \approx 0.15$ , are still preserved 40 ns after the load was released, see Fig. 11.

The system structure is visualized in a series of snapshots taken at various relevant time instants, see Fig. 12. A snapshot taken at 16 ns displays the stretched isotropic phase, whereas those at 25 ns and 48 ns indicate that the ordered phase with  $S_y \approx 0.4$  is a polydomain smectic. Domain directors are distributed within the XY plane with preference given to the Y axis. This is the consequence of a biaxial symmetry imposed on the mesogens by the uniaxial load. Indeed, a negative backbone–mesogen coupling is expected to force the mesogens to stay predominantly perpendicular to the Z axis, and then the symmetry within the XY plane is broken by the orientational ordering. This situation bears much similarity to the photo-reorientation of azobenzenes.<sup>26</sup> After the load is released, the structure of the LCE turns back to being almost isotropic, as discussed above, this is displayed in the snapshot taken at  $t = 90$  ns.

### B. Sm A phase: uniform and stripe-patterned director reorientation

The monodomain smectic-A LCE sample is characterized by a lamellar structure with alternation of the LC and polymer layers, see Fig. 2. The backbones are spatially restricted within polymer-rich layers and have an oblate shape with respect to the nematic director. This is supported by an estimate for the ratio between gyration radii parallel and perpendicular to the director, which for our model smectic LCE is  $R_{\parallel}/R_{\perp} \approx 0.4$ . Therefore, application of a sufficient load parallel to the director is expected to result in massive conformational changes of backbone shape from oblate to prolate in the direction of the load. As a result, the LC order is perturbed due to coupling between backbone and mesogens. A number of scenarios for these changes have been observed experimentally.<sup>35,42,43,48,49</sup> The elastic modulus of the smectic LCE normal to the director is about two orders of magnitude smaller than the modulus parallel to the director.<sup>42</sup> Therefore, the sample can be easily stretched perpendicularly to the director (*i.e.* within the plane of the layers) and withstands deformations of at least 200%. It is worth noting that such a

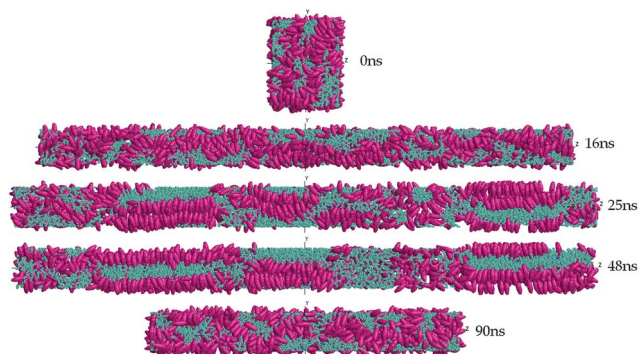


**Fig. 12** Snapshots illustrating the stages in formation of the stress-induced polydomain smectic phase in the isotropic LCE at  $T = 510$  K (see Fig. 11). The amount of load is  $P_L = 37$  atm, and the time elapsed since the creep starts is indicated in the figure.

deformation preserves both the order of the mesogens in the respective layers and the dimensions of the sample along the director.<sup>42</sup>

In this subsection we present the results of a creep experiment applied to both the model systems (LCP melt and LCE) in the monodomain smectic phase in a range of temperatures from 480 K to 500 K. Let us concentrate first on the case when the uniaxial load is applied parallel to the director (along the  $Z$  axis). Some typical cases for the evolution of the deformation  $\epsilon = L_z(t)/L_z(0)$  upon application of a load with different values of  $P_L$  are shown in Fig. 13. One can distinguish four principal stages of deformation:

- stage 1*: initial regime with constant strain,
- stage 2*: transition-like rapid shape transformation,
- stage 3*: plateau region,
- stage 4*: fracturing of the sample.

For the case of the LCP melt, typically, only *stage 1* and *stage 4* are observed (see Fig. 13, left frame). At the end of *stage 4*, the sample disintegrates. The flat part of *stage 1*, estimated for the case of  $P_L = 31$  atm, is characterized by a deformation of about 6%, whereas fracturing occurs at deformations higher than 20%. Similar behavior is found for the LCE at high loads,  $P_L \geq 64$  atm (see Fig. 13, right frame), where fracturing occurs at

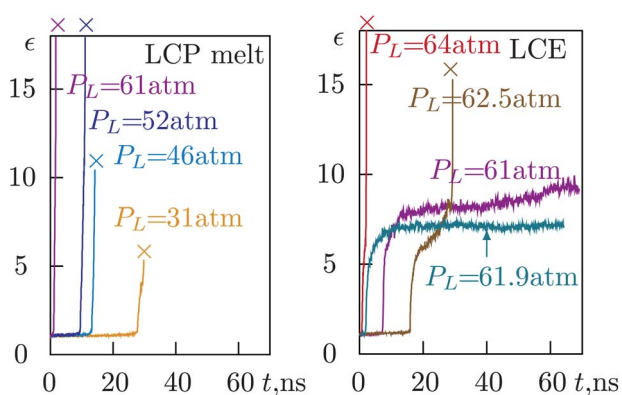


**Fig. 13** Evolution of the deformation  $\epsilon$  along the stretch axis  $Z$  for the monodomain smectic samples of LCP melt and LCE at 500 K. The load of various strengths  $P_L$  is applied parallel to the initial nematic director.

deformations of about 700%. With the decrease of  $P_L$  below a certain threshold value, *stage 2* and *stage 3* start to develop before fracturing takes place (see the case of  $P_L = 62.5$  atm for the LCE). With a further decrease of load down to  $P_L = 61.9$  atm and below, the time intervals for *stage 1* and *stage 3* both increase. In this case, a plateau region (*stage 3*) of at least 60 ns duration is found. This sample, after being stretched to 800–900% along the initial director, demonstrated remarkable elasticity. One may suggest that such high elasticity is the result of the interlayer links formed by two backbones (see Fig. 2, image (c)). The existence of such links has been suggested in some experimental studies (see Fig. 3 in ref. 43). Similar plateau regions for the strain are also observed for the sample LCE[480-1] (discussed below). One should note that *stage 2* and *stage 4* are always found to occur on rather short time scales (transition-like changes).

We will discuss below the results obtained at  $T = 480$  K. The same behavior is observed for all temperatures up to 500 K; the only difference is in the threshold value  $P'_L$ , which decreases at higher temperatures. This can be attributed to a weakening of the LC interaction. The exact time scale and microscopic scenario, however, is found to depend strongly on the preparation history of the system, at least for the system sizes considered in our study. As an illustration, we present the results obtained for two LCE samples, LCE[480-1] and LCE[480-2] with different thermal histories. In the case of LCE[480-1], a freshly made network crosslinked at 450 K (see Section II) is first equilibrated at the same temperature for 27.2 ns, and then heated up to 480 K for another 23.3 ns. For preparation of LCE[480-2], the same fresh network was first heated to 500 K for 17.6 ns and then cooled down to 480 K for another 22.9 ns.

The load of  $P_L = 73$  atm is applied first to the LCE[480-1] sample parallel to the nematic director. As a result, the backbone anisotropy  $R_{||}/R_{\perp}$  and the LC order parameters  $S_x$ ,  $S_y$  and  $S_z$ , undergo the changes shown in Fig. 14. During *stage 1* (1–10 ns),  $R_{||}/R_{\perp}$  changes gradually from an initial value of 0.4 to approximately 1, whereas  $S_z$  decreases from 0.75 to 0.55–0.6 and  $S_x$  increases from  $-0.34$  to  $-0.1$ . At  $t = 10$  ns the system undergoes the *stage 2* transformation characterized by a jump of  $R_{||}/R_{\perp}$  up to 5 and rapid exchange of the values between  $S_z$  and  $S_x$  which indicates director reorientation. The threshold value of

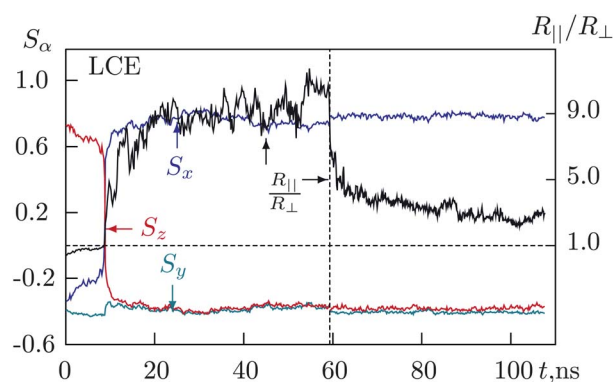


**Fig. 14** Nematic order parameter  $S_\alpha$  along each spatial axis  $\alpha$  and the backbone anisotropy  $R_{||}/R_{\perp}$  at load  $P_L = 73$  atm, applied along the  $Z$  axis, to a monodomain smectic sample LCE[480-1] at  $T = 480$  K.

$R_{\parallel}/R_{\perp}$ , at which this transformation starts, is about 1.2–1.25. The state with rotated nematic director initiated in *stage 2* is matured during *stage 3*, where  $R_{\parallel}/R_{\perp}$  increases further up to about 9–10, but no essential change in LC order takes place. The LCE[480-1] sample is found to be stable under the load of  $P_L = 73$  atm at least for 60 ns time; therefore, no *stage 4* is observed within the time window of our simulation. After application of the load for 60 ns it was released and, as a result, the backbone anisotropy decreased after 45 ns down to  $R_{\parallel}/R_{\perp} \approx 2.5$ ; this value is exactly the reciprocal of the initial one equal to 0.4. Therefore, the initial smectic phase is reoriented uniformly under a load applied parallel to the initial nematic director, and the resulting phase has the same properties (in terms of backbone anisotropy and the nematic order parameter) but with the director being rotated by  $90^\circ$ . The snapshots illustrating uniform director reorientation are presented in Fig. 15. The snapshots also confirm the integrity of the sample at all stages. One can also note that at an early stage of director reorientation ( $t < 8.6$  ns) the load somewhat reduces the layered structure defects in the smectic sample upon rotation of the director.

In the second simulation, we applied the same load  $P_L = 73$  atm to the same LCE[480-1] sample, *perpendicularly* to the nematic director, along the  $Y$  axis. Typical real samples are found to stay transparent up to high strains of 200%, and to preserve their initial width in the direction of the layer normal.<sup>42</sup> This means that the degree of LC order, the director orientation and the sample width along the director stay unchanged. All these results are found in the simulation of our model system. In particular, a strain of 230% is developed along the load axis ( $Y$ ). More details of microscopic changes in the sample are presented in Fig. 16. The backbone anisotropy along the  $Y$  axis increases up to  $R_{\parallel}/R_{\perp} \approx 4$ . The order parameters  $S_x$ ,  $S_y$ ,  $S_z$  and relative elongation  $\epsilon$  along the  $Z$  axis (parallel to the director) do not change, confirming the experimental results. After the load is released at  $t = 26.5$  ns, the backbone anisotropy decreases gradually towards a residual value of  $R_{\parallel}/R_{\perp} \approx 1.5$ . The residual strain along the  $Y$  axis is about 140%.

Let us switch now to the second smectic sample, LCE[480-2]. A load of the same strength,  $P_L = 73$  atm, is applied at the same

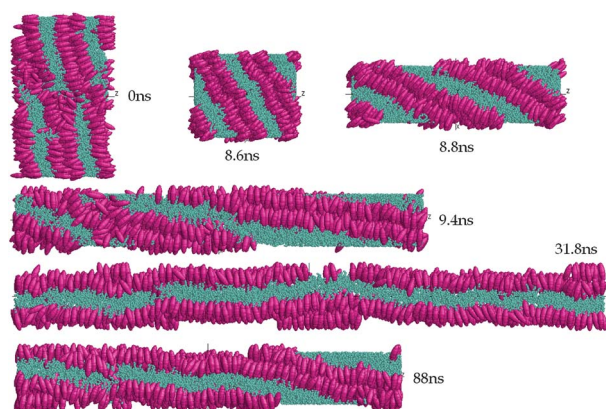


**Fig. 15** Snapshots illustrating the stages of uniform director reorientation upon application of a uniaxial load  $P_L = 73$  atm along the  $Z$  axis (parallel to the director and to the layer normal) to a monodomain smectic sample LCE[480-1] at  $T = 480$  K (see Fig. 14).

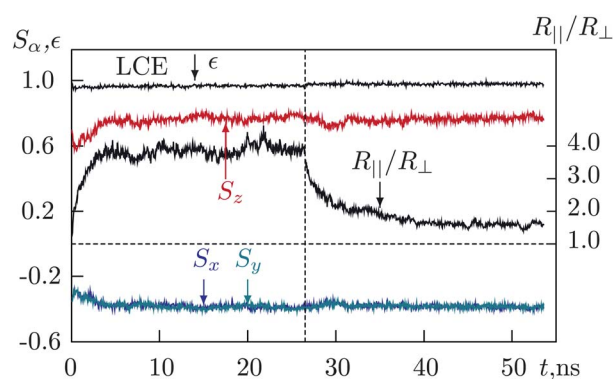


**Fig. 16** Nematic order parameter  $S_\alpha$  along each spatial axis  $\alpha$ , backbone anisotropy  $R_{\parallel}/R_{\perp}$  with respect to load axis, and relative elongation  $\epsilon$  of the sample along the director axis. The load of  $P_L = 73$  atm is applied along the  $Y$  axis (perpendicular to the director) to a monodomain smectic sample LCE[480-1] at  $T = 480$  K.

temperature,  $T = 480$  K, along the  $Z$  axis (parallel to the director). The sample develops a stripe-like director pattern (with only two stripes within a single periodic box) during the first 1.5–2 ns, but in 4 ns time this fractures, as shown in Fig. 17. One must mention that the monodomain smectic samples, LCE[480-1] and LCE[480-2], differ only in their thermal history, having a similar defect in their structure before the load is applied (see Fig. 15 and 17). However, radically different director responses are found in these samples upon application of the same amount and direction of load. In particular, the sample LCE[480-1] demonstrates a gradual reorientation of the director, whereas LCE[480-2] develops a stripe-like pattern under load. As follows from the snapshots presented in Fig. 15, the layer normal for the LCE[480-1] sample at  $t = 0$  is not exactly parallel to the  $Z$  axis. Therefore, the results obtained in our simulations can be related to the experiments performed on nematic LCEs when the direction of the applied load is not exactly perpendicular to the director. In this case, gradual director reorientation is found.<sup>35,36</sup> The sample LCE[480-2] at  $t = 0$  demonstrates two smectic regions with slightly different angles between their respective layer normals

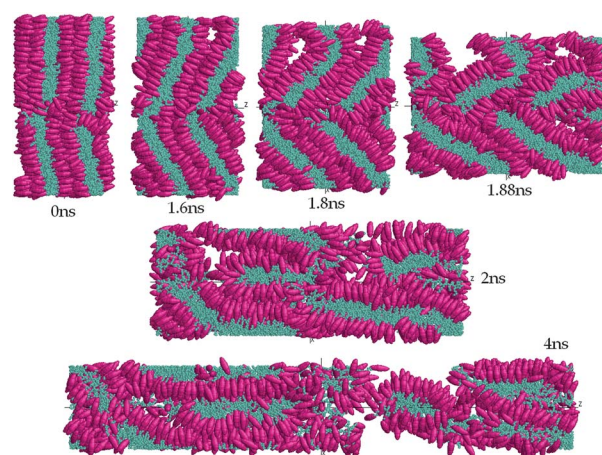


**Fig. 17** Series of snapshots taken at characteristic times to illustrate the stretching of the LCE[480-2] sample at 480 K with a load  $P_L = 73$  atm applied along the director.

and Z axis. The formation of a stripe-like pattern can be explained in two possible ways. The first explanation is that the layer normal averaged over the sample volume is parallel to the Z axis. Then, this case is similar to the experiments on nematic LCEs when the load is applied perpendicular to the director, and stripe formation is also observed.<sup>23</sup> The second explanation could be the presence of the defect which separates the two smectic regions in the initial configuration. Upon application of the load, the directors in each region rotate independently, which results in a V-shaped or chevron-like structure. Indeed, the wedge of this pattern is developed exactly at the defect position. As follows from these simulations, both thermal history and, possibly, the existing defects in structure play an important role in the kind of response developed under the load. Similar remarks on the role of the preparation history of the sample on its behavior under stress were made earlier, in the experimental work by Zhang *et al.*<sup>51</sup> These results lead us to believe that the simulations are correctly embodying the essential physics, but our model system is rather small to be able to study periodic stripe formation as found experimentally,<sup>23,35,37,42,43,47–49</sup> and discussed theoretically.<sup>45,50</sup>

## VI. Conclusions

We have performed extensive molecular dynamics simulations aimed to reproduce the principal features of LC elastomers of side-chain architecture. To the best of our knowledge, this is the first atom-based molecular dynamics simulation of such systems described by a force-field model. We developed an algorithm for crosslinking of the melt, which allows us to achieve a uniform spatial distribution of crosslinks. The elastomer is formed by crosslinking of the melt in the smectic A phase. Following equilibration, this is subsequently driven through the smectic–isotropic transition, and memory effects are studied. We also studied the influence of a uniaxial load applied both above and below the smectic–isotropic transition point.

A number of experimentally observed effects are reproduced, namely:

- an increase of the smectic–isotropic temperature of about 5 degrees due to crosslinking;
- high elasticity of the elastomer in the isotropic phase in a creep experiment;
- memory effects in liquid-crystalline order and sample shape, when the elastomer is driven through the smectic–isotropic transition;
- a stress-induced smectic phase by uniaxial stretching of the isotropic sample;
- stress-induced uniform director reorientation and stripe-like deformation of the smectic structure upon uniaxial stretch of a monodomain smectic sample along the director.

The ultimate aim of this type of simulation is the prediction of the way the mechanical response of this class of functional materials depends on their chemical architecture, and this study is a first step towards this goal. It can be extended in several directions. Firstly, larger system sizes can be considered to investigate stripe-like deformations of the director in detail. For this purpose it is reasonable to use moderately coarse-grained molecular dynamics or similar approaches, investigate carefully the effects of finite system size, and make contact with continuum

theories. Secondly, one can extend the simulations to cover the case of photo-deformable (*e.g.* azobenzene-containing) elastomers<sup>7,84,85</sup> of the kind that might be used in artificial muscles.

## Acknowledgements

The authors acknowledge financial support under DFG Grant NE410/8-2 and GR 3725/2-1.

## References

- 1 *Thermotropic Liquid Crystalline Polymers*, ed. T. S. Chung, Technomic: Lancaster, PA, 2001.
- 2 M. Warner and E. M. Terentjev, *Liquid Crystal Elastomers*, Oxford University Press, 2007.
- 3 M. Behl and A. Lendlein, *Mater. Today*, 2007, **10**, 20.
- 4 S. Ahn, P. Deshmukh, M. Gopinadhan, C. O. Osuji and R. M. Kasi, *ACS Nano*, 2011, **5**, 3085.
- 5 D. K. Shenoy, D. L. Thomsen, A. Srinivasan, P. Keller and B. R. Ratna, *Sens. Actuators, A*, 2002, **96**, 184.
- 6 C. M. Spillman, J. Naciri, B. D. Martin, W. Farahat, H. Herr and B. R. Ratna, *Sens. Actuators, A*, 2007, **133**, 500.
- 7 T. Ikeda, J. Mamiya and Y. Yu, *Angew. Chem., Int. Ed.*, 2007, **46**, 506.
- 8 A. J. Symons, F. J. Davis and G. R. Mitchell, *Liq. Cryst.*, 1993, **14**, 853.
- 9 A. J. Symons, F. J. Davis and G. R. Mitchell, *Polymer*, 1999, **40**, 5365.
- 10 F. J. Davis and G. R. Mitchell, *Polymer*, 1996, **37**, 1345.
- 11 M. Warner, K. P. Gelling and T. A. Vilgis, *J. Chem. Phys.*, 1988, **88**, 4008.
- 12 C. H. Legge, F. J. Davis and G. R. Mitchell, *J. Phys. II*, 1991, **1**, 1253.
- 13 J. Schätzle, W. Kaufhold and H. Finkelmann, *Makromol. Chem.*, 1989, **190**, 3269.
- 14 N. Assfalg and H. Finkelmann, *KGK, Kautsch. Gummi Kunstst.*, 1999, **52**, 677.
- 15 A. R. Tajbakhsh and E. M. Terentjev, *Eur. Phys. J. E: Soft Matter Biol. Phys.*, 2001, **6**, 181.
- 16 H. Hirschmann, P. M. S. Roberts, F. J. Davis, W. Guo, C. D. Hasson and G. R. Mitchell, *Polymer*, 2001, **42**, 7063.
- 17 P. E. Cladis, *Proc. EuroMech408*, ed. P. Ehrhard and D. Riley, Kluewer Academic, 2001, p. 123.
- 18 M. Warner and E. Terentjev, *Macromol. Symp.*, 2003, **200**, 81.
- 19 G. R. Mitchell, F. J. Davis, W. Guo and R. Cywinski, *Polymer*, 1991, **32**, 1347.
- 20 R. G. Kirste and H. G. Ohm, *Makromol. Chem., Rapid Commun.*, 1985, **6**, 179.
- 21 P. Keller, B. Carvalho, J. P. Cotton, M. Lambert, I. Moussa and C. Pepy, *J. Phys.*, 1985, **46**, L1065.
- 22 G. R. Mitchell, M. Coulter, F. J. Davis and W. Guo, *J. Phys. II*, 1992, **2**, 1121.
- 23 J. Küpfer and H. Finkelmann, *Makromol. Chem., Rapid Commun.*, 1991, **12**, 717.
- 24 J. M. Ilynyskiy and D. Neher, *J. Chem. Phys.*, 2007, **126**, 174905.
- 25 J. M. Ilynyskiy, D. Neher and M. Saphiannikova, *Condens. Matter Phys.*, 2006, **9**, 87.
- 26 J. M. Ilynyskiy, D. Neher and M. Saphiannikova, *J. Chem. Phys.*, 2011, **135**, 044901.
- 27 G. H. F. Bergmann, H. Finkelmann, V. Percec and M. Zhao, *Macromol. Rapid Commun.*, 1997, **18**, 353.
- 28 H. Finkelmann and H. Wermter, ACS Abstracts 219, 189-PMSE pt. 2, 2000.
- 29 H. Finkelmann, H. J. Koch and G. Rehage, *Makromol. Chem., Rapid Commun.*, 1981, **2**, 317.
- 30 H. Finkelmann, H.-J. Kock, W. Gleim and G. Rehage, *Makromol. Chem., Rapid Commun.*, 1984, **5**, 287.
- 31 G. R. Mitchell, F. J. Davis and A. S. Ashman, *Polymer*, 1987, **28**, 639.
- 32 C. Degert, P. Davidson, S. Megtert, D. Petermann and M. Mauzac, *Liq. Cryst.*, 1992, **12**, 779.
- 33 G. R. Mitchell, F. J. Davis and W. Guo, *Phys. Rev. Lett.*, 1993, **71**, 2947.
- 34 J. Küpfer and H. Finkelmann, *Macromol. Chem. Phys.*, 1994, **195**, 1353.
- 35 I. Kundler and H. Finkelmann, *Macromol. Rapid Commun.*, 1995, **16**, 679.

- 36 P. M. S. Roberts, G. R. Mitchell, F. J. Davis and J. A. Pople, *Mol. Cryst. Liq. Cryst.*, 1997, **299**, 181.
- 37 G. C. Verwey, M. Warner and E. M. Terentjev, *J. Phys. II*, 1996, **6**, 1273.
- 38 M. Warner and E. M. Terentjev, *Prog. Polym. Sci.*, 1996, **21**, 853.
- 39 P. Bladon, E. M. Terentjev and M. Warner, *Phys. Rev. E: Stat. Phys., Plasmas, Fluids, Relat. Interdiscip. Top.*, 1993, **47**, 3838.
- 40 P. Bladon, M. Warner and E. M. Terentjev, *Macromolecules*, 1994, **27**, 7067.
- 41 J. Weilepp and H. R. Brand, *Europhys. Lett.*, 1996, **34**(7), 495.
- 42 E. Nishikawa and H. Finkelmann, *Macromol. Rapid Commun.*, 1997, **18**, 65.
- 43 E. Nishikawa and H. Finkelmann, *Macromol. Chem. Phys.*, 1999, **200**, 312.
- 44 O. Stenull and T. C. Lubensky, *Phys. Rev. E: Stat., Nonlinear, Soft Matter Phys.*, 2007, **76**, 011706.
- 45 J. M. Adams and M. Warner, *Phys. Rev. E: Stat., Nonlinear, Soft Matter Phys.*, 2005, **71**, 021708.
- 46 J. M. Adams and M. Warner, *Phys. Rev. E: Stat., Nonlinear, Soft Matter Phys.*, 2008, **77**, 021702.
- 47 J. S. Biggins, *Liq. Cryst.*, 2009, **36**, 1139.
- 48 I. Kundler and H. Finkelmann, *Macromol. Chem. Phys.*, 1998, **199**, 677–686.
- 49 H. Finkelmann, I. Kundler, E. M. Terentjev and M. Warner, *J. Phys. II*, 1977, **7**, 1059.
- 50 E. Fried and S. Sellers, *J. Appl. Phys.*, 2006, **100**, 043521.
- 51 F. Zhang, P. A. Heiney, A. Srinivasan, J. Naciri and B. Ratna, *Phys. Rev. E: Stat., Nonlinear, Soft Matter Phys.*, 2006, **73**, 021701.
- 52 W. Zhu, M. Shelley and P. Palfy-Muhoray, *Phys. Rev. E: Stat., Nonlinear, Soft Matter Phys.*, 2011, **83**, 051703.
- 53 J. V. Selinger, H. G. Jeon and B. R. Ratna, *Phys. Rev. Lett.*, 2002, **89**, 225701.
- 54 J. V. Selinger and B. R. Ratna, *Phys. Rev. E: Stat., Nonlinear, Soft Matter Phys.*, 2004, **70**, 041707.
- 55 P. Pasini, G. Skačej and C. Zannoni, *Chem. Phys. Lett.*, 2005, **413**, 463.
- 56 G. Skačej and C. Zannoni, *Eur. Phys. J. E: Soft Matter Biol. Phys.*, 2008, **25**, 181–186.
- 57 A. Darinskii, A. Zarembo, N. K. Balabaev, I. M. Neelov and F. Sundholm, *Macromol. Symp.*, 2006, **237**, 119.
- 58 A. Darinskii, A. Zarembo and N. K. Balabaev, *Macromol. Symp.*, 2007, **252**, 101.
- 59 G. Skačej and C. Zannoni, *Soft Matter*, 2011, **7**, 9983.
- 60 G. Skačej and C. Zannoni, *Proc. Natl. Acad. Sci. U. S. A.*, 2012, **109**, 10193.
- 61 J. Ilynyskiy and M. R. Wilson, *Comput. Phys. Commun.*, 2001, **134**, 23.
- 62 J. Ilynyskiy and M. R. Wilson, *Comput. Phys. Commun.*, 2002, **148**, 43.
- 63 R. Hill, *Math. Proc. Cambridge Philos. Soc.*, 1984, **95**, 481; *J. Int. Biomed. Inf. Data*, 1985, **98**, 579.
- 64 K. Matouš and P. H. Geubelle, *Int. J. Numer. Meth. Eng.*, 2006, **65**, 190.
- 65 A. Aharony and A. Brooks Harris, *Phys. Rev. Lett.*, 1996, **77**, 3700; K. Binder and A. P. Young, *Rev. Mod. Phys.*, 1986, **58**, 801; S. Wiseman and E. Domany, *Phys. Rev. E: Stat. Phys., Plasmas, Fluids, Relat. Interdiscip. Top.*, 1998, **58**, 2938.
- 66 J. C. Michel, H. Moulinec and P. Suquet, *Comput. Meth. Appl. Mech. Eng.*, 1999, **172**, 109.
- 67 M. R. Wilson, *J. Chem. Phys.*, 1997, **107**, 8654.
- 68 J. G. Gay and B. J. Berne, *J. Chem. Phys.*, 1981, **74**, 3316.
- 69 C. McBride and M. R. Wilson, *Mol. Phys.*, 1999, **97**, 511.
- 70 M. R. Wilson, J. M. Ilynyskiy and L. M. Stimson, *J. Chem. Phys.*, 2003, **119**, 3509.
- 71 M. R. Wilson, J. M. Ilynyskiy, L. M. Stimson and Z. E. Hughes, in *Computer Simulations of Liquid Crystals and Polymers*, ed. P. Pasini, C. Zannoni and S. Zumer, Kluwer, 2004, p. 57.
- 72 L. M. Stimson and M. R. Wilson, *J. Chem. Phys.*, 2005, **123**, 034908.
- 73 M. R. Wilson, L. M. Stimson and J. M. Ilynyskiy, *Liq. Cryst.*, 2006, **33**, 1167.
- 74 J. M. Ilynyskiy, D. Neher, M. Saphiannikova, M. R. Wilson and L. M. Stimson, *Mol. Cryst. Liq. Cryst.*, 2008, **496**, 186.
- 75 J. M. Ilynyskiy, D. Neher and M. Saphiannikova, in *CP1091, Modeling and Simulation of New Materials: Tenth Granada Lectures*, ed. P. L. Garrido, P. I. Hurtago and J. Marro, AIP, 2009.
- 76 M. Parrinello and A. Rahman, *J. Appl. Phys.*, 1981, **52**, 7182.
- 77 L. Penna, D. Catalano and C. A. Veracini, *J. Chem. Phys.*, 1996, **105**, 7097.
- 78 A. Cuetos, J. M. Ilynyskiy and M. R. Wilson, *Mol. Phys.*, 2002, **100**, 3839.
- 79 P. J. Collings and M. Hird, *Introduction to Liquid Crystals*, Taylor and Francis, 2001.
- 80 G. R. Bakhshandeh and J. E. Stuckey, *Iran. J. Polym. Sci. Technol.*, 1992, **1**, 25.
- 81 M. Klüppel, *J. Appl. Polym. Sci.*, 1993, **48**, 1137.
- 82 V. M. Litvinov and P. P. De, *Spectroscopy of Rubber and Rubbery Materials*, Rapra Technology Ltd., 2002, vol. 654, p. 360.
- 83 W. Ren, P. J. McMullan and A. C. Griffin, *Macromol. Chem. Phys.*, 2008, **209**, 1896.
- 84 V. Toshchevikov, M. Saphiannikova and G. Heinrich, *J. Phys. Chem. B*, 2012, **116**, 913.
- 85 V. Toshchevikov, M. Saphiannikova and G. Heinrich, *J. Chem. Phys.*, 2012, **137**, 024903.